

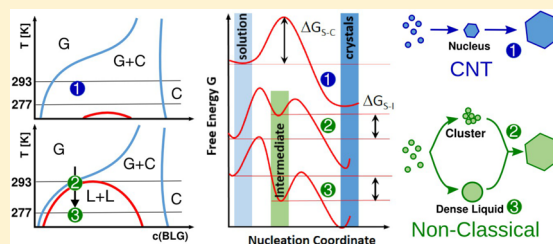
Nonclassical Pathways of Protein Crystallization in the Presence of Multivalent Metal Ions

Andrea Sauter,[†] Melanie Oelker,[‡] Georg Zoicher,[‡] Fajun Zhang,^{*,†} Thilo Stehle,^{*,‡,#} and Frank Schreiber[†][†]Institut für Angewandte Physik, Universität Tübingen, Auf der Morgenstelle 10, 72076 Tübingen, Germany[‡]Interfakultäres Institut für Biochemie, Universität Tübingen, Hoppe-Seyler-Straße 4, 72076 Tübingen, Germany[#]Department of Pediatrics, Vanderbilt University School of Medicine, Nashville, Tennessee 37232, United States

S Supporting Information

ABSTRACT: Using bovine β -lactoglobulin as a model system, we have studied the crystallization pathways in the presence of the di- and trivalent salts ZnCl_2 and YCl_3 . Previous work has shown that protein solutions undergo a reentrant condensation (RC) phase behavior in the presence of YCl_3 , i.e., a condensed phase occurs in between two boundary salt concentrations, $c^* < c^{**}$. In the presence of ZnCl_2 , c^* also exists, but protein solutions with high salt concentrations do not become completely clear at higher protein concentrations (>20 mg/mL). We thus denote this diffuse transition as *pseudo- c^{**}* . Small angle

X-ray scattering measurements show that the effective interactions change from repulsion to attraction near c^* , and attractive interactions dominate around *pseudo- c^{**}* . Solutions near c^* and *pseudo- c^{**}* provide the optimized conditions for growth of high quality protein single crystals but with different pathways. While crystal growth near c^* follows the classical one-step nucleation pathway, crystallization around *pseudo- c^{**}* (for zinc) or c^{**} (for yttrium) follows a nonclassical process with an intermediate phase appearing before crystallization. Furthermore, the intermediate phases strongly depend on the crystallization temperature. Samples with high salt concentrations exhibit a typical transition temperature, T_{tr} , below which the solutions become turbid. When crystallizing near T_{tr} , the intermediate phase consists of protein clusters; below T_{tr} , the intermediate phase corresponds to macroscopic protein aggregates which can further relax into a dense liquid phase before crystallization. However, the experimental data cannot distinguish whether nucleation occurs within or outside of the intermediate phase. Possible scenarios are discussed based on the equilibrium phase behavior of colloidal systems with a short-range attraction. The crystallographic analysis of the resulting crystals shows that metal ions are an integral part of the crystal lattice. Both types of metal ions can create new protein contacts in the crystal lattice via bridging; however, yttrium creates more bridging contacts compared to zinc.



■ INTRODUCTION

Crystallography is the dominating method for structure determination of biological macromolecules. Its major bottleneck is the crystallization from protein solutions and growing single crystals with adequate quality. The molecular interactions in protein solutions, in particular their connection to the crystallization process, are not completely understood, and crystal growth is typically performed by trial and error experiments.¹

Recent progress in protein and colloid crystallization as well as biomineralization has shown nonclassical features in the early stage of nucleation.^{2–6} While classical nucleation theory (CNT) predicts that molecules form nuclei in a supersaturated solution with the exact density and structure of the crystals in the final stage,^{4,7,8} nonclassical pathways suggest an intermediate phase (clusters or dense liquid phase) existing in between the initial solution and the final crystalline state.^{2–4,6} The free energy landscapes of nonclassical pathways show an additional free energy minimum corresponding to the intermediate phase. Computer simulations of homogeneous crystal nucleation performed by ten Wolde and Frenkel using a colloidal model with short-range attractive interactions suggested that the

presence of large density fluctuations close to the critical point of liquid–liquid phase separation (LLPS) affects the pathway for the formation of a crystal nucleus.² The free-energy barrier that has to be overcome is considerably lowered if the change in density occurs before the structural change.² While the theoretically predicted two-step nucleation near the critical point is difficult to verify experimentally, accumulated experimental observations in various systems have shown the nonclassical features of crystallization under certain conditions.^{3,9–12} Even in simple hard-sphere systems, simulations and experiments suggest a two-step nucleation process with amorphous clusters as precursors.^{13–17}

A different type of cluster phase has been proposed for concentrated protein solutions that is not caused by density fluctuations: Large clusters consisting of 10^5 to 10^6 proteins have been observed in lysozyme and hemoglobin systems outside the LLPS region.^{18–20} An approach to find an electrostatic model for clusters with up to 10^3 molecules was

Received: July 22, 2014

Revised: October 7, 2014

Published: October 29, 2014

pursued by Hutchens and Wang.²¹ This model is, however, limited by the Debye screening length and cannot explain the experimentally observed large clusters. Nevertheless, these large protein clusters have been demonstrated to play an important role in the protein crystallization process which cannot be explained by CNT.^{18–20,22,23}

In practice, an occasionally used and successful strategy to induce protein crystallization is the addition of multivalent ions.^{24–27} Divalent ions have been proven crucial for the generation of high quality crystals of insulin and other protein complexes.^{28,29} We have shown previously that trivalent salts such as YCl_3 can induce a reentrant condensation (RC) phase behavior in many acidic proteins such as β -lactoglobulin (BLG).^{30–34} For a given protein concentration, when the salt concentration is below c^* and/or above c^{**} , protein solutions are clear. At salt concentrations between c^* and c^{**} (with $c^* < c^{**}$), protein condensation occurs including aggregation, LLPS, and crystallization.^{35,36} Interestingly, depending on the position in the phase diagram, classical crystallization or a temperature-dependent nonclassical crystallization process has been observed.³⁶ Further studies suggested that proteins form clusters in the presence of trivalent metal ions that can form either a dense liquid phase or crystals depending on the kinetics.^{34,37} However, establishing a complete picture of the nucleation mechanism in the presence of the metastable intermediate phase and its role is still a challenge.

In this work, we aim to provide new insights into the nonclassical pathways for protein crystallization in the presence of multivalent metal ions. We first determine and compare the macroscopic phase behavior and crystal growth pathways for BLG with a trivalent salt, YCl_3 , and a divalent salt, ZnCl_2 . We further characterize the effective protein–protein interactions in the molecular level using small-angle X-ray scattering. Finally, we explore the role of multivalent metal ions based on the high resolution crystal structure on the atomic level. We hypothesize that the difference in valency will lead to a different binding affinity of the metal ions to the protein surface,³⁸ which may affect the resulting crystal lattice and the kinetics of crystal growth. By providing more detailed experimental observations of crystal growth under various conditions and the structural analysis of the protein crystals, we aim to address the following questions: Which crystallization pathways are followed and what is the structure and morphology of the crystals? What is the role of multivalent ions in stabilizing the crystal lattice as well as inducing the different pathways of crystallization? Are there differences between ZnCl_2 and YCl_3 , concerning the pathway of crystallization and the ion-bridging?

■ EXPERIMENTAL SECTION

Materials and Sample Preparation. Protein and salts were purchased from Sigma-Aldrich. The guaranteed purities were 90% for BLG from bovine milk (L3908), 97% for ZnCl_2 (96468), and 99.99% for YCl_3 (451363). A BLG monomer consists of 162 amino acids and has a molecular mass of about 18.3 kDa. Under physiological conditions, it is found predominantly as a dimer.³⁹ With an isoelectric point (pI) of 5.2, it is acidic and carries a net charge of $-10 e$ at neutral pH.⁴⁰ All samples were prepared by mixing the required amount of salt stock solution, deionized (18.2 M Ω) degassed Millipore water and protein stock solution. Stock solutions were prepared by dissolving the protein powder or salt in deionized degassed Millipore water. The concentration of BLG solutions was determined by UV absorption measurements using an extinction coefficient of $0.96 \text{ l} \cdot \text{g}^{-1} \cdot \text{cm}^{-1}$ at a wavelength of 278 nm.⁴¹ A Seven Easy pH instrument from Mettler Toledo was used to monitor the pH of protein solutions caused by salt

addition. All samples had a pH above the pI (between 6.2 and 6.9). Since most buffers can affect the phase behavior and the solubility of salts, no additional buffer was used to avoid the effect of cosalts.

The transition temperature, T_{tr} , for samples with high salt concentration was determined by turbidity measurements. Samples were prepared in a water bath at 313 K and then slowly cooled to 278 K with a cooling rate of about 0.1 K/min. Pictures were taken every 2 K, and the temperature of the transition from clear to turbid was assigned as T_{tr} .

Methods. Small Angle X-ray Scattering (SAXS) and Data Analysis. SAXS measurements were performed at the ESRF, Grenoble, France, at beamline ID02. The samples were measured using a flow-through capillary cell with a thickness of about $10 \mu\text{m}$ at sample-to-detector distances of 1, 2, and 5 m. The sample in the scattering volume was exchanged for every exposure. For each sample, 10 exposures of 0.1 s or 20 exposures of 0.05 s each were measured. The two-dimensional (2D) intensity pattern was corrected to an absolute scale and azimuthally averaged to obtain the intensity profiles. Afterward, the solvent background was subtracted. More detailed information on data reduction and q -resolution calibration can be found in the literature.^{42,43}

Small-angle X-ray scattering data can be used to obtain information on the pair interaction potential.^{44–46} The scattering intensity, $I(q)$, for a nonspherical system, can be expressed by

$$I(q) = N(\Delta\rho)^2 V^2 P(q) \bar{S}(q) \quad (1)$$

where $q = ((4\pi)/(\lambda)) \sin(\theta/2)$ is the scattering vector, θ is the scattering angle, N is the number of protein molecules per unit volume in the solution, $\Delta\rho = \rho_p - \rho_s$ is the electron density difference between the solvent and the solute, and V is the volume of a single protein. $P(q)$ is the form factor of a given protein, i.e., the scattering from a single protein molecule after orientation averaging. A form factor of an oblate ellipsoid with semiaxes a and b is used to model the protein BLG. At low protein and salt concentration, the SAXS data were fitted by the crystal structure of the BLG dimer (PDB code of 1BE6⁴⁷) using CRY SOL.⁴⁸ The structure factor $\bar{S}(q)$ is calculated using the average structure factor approximation from a monodisperse spherical system,⁴⁹ with an effective sphere diameter which is calculated from a virtual sphere with the same second virial coefficient as the ellipsoid.^{37,50} In the following parts and for simplicity, we use $S(q)$ to denote $\bar{S}(q)$. To describe the effective interactions in protein solution, structure factors derived from model potentials were used for data analysis. Data fitting for the determination of the interaction potential was performed on IGOR PRO with macros developed at NIST.⁵¹ More details of data analysis can be found in previous work.^{43,52}

Protein Crystallization and Crystal Structure Analysis. Crystallization was performed at 277, 293, and 312 K by the vapor diffusion hanging drop method or by batch crystallization in small glass bottles or cuvettes. The concentrations ranged from 3 to 65 mg/mL BLG and 0–50 mM ZnCl_2 or 0–20 mM YCl_3 , respectively. The crystallization process was followed with transmission optical microscopes: a KL 1500 LCD from Leica Microsystems Inc. in a 293 K room, an Axioskop 40 from Zeiss with an installed Nikon E995 digital camera in a 277 K room and an AxioScope.A1 from Zeiss with an included AxioCam ICC5, temperature-controlled by a water bath with a precision of 0.05 K.

X-ray analysis was performed with two typical crystals from different regions of the phase diagram (BLG-Zn-2: 10.0 mg/mL BLG and 2 mM ZnCl_2 ; BLG-Zn-20: 3.4 mg/mL BLG and 20 mM ZnCl_2) both grown at 277 K. Single crystals were prepared and transferred into the corresponding salt concentration including glycerol (30–34% (w/v)). The crystals were flash frozen in liquid nitrogen and stored until data collection. Data collection was performed at beamlines X06DA at the Swiss Light Source in Villigen, Switzerland, and P13 at PETRA III in Hamburg, Germany. Data processing was performed with the XDS package.⁵³ Structures were solved by molecular replacement as implemented in PHASER⁵⁴ using coordinates for BLG (Protein Data Bank (PDB) code 3PH5) as search template, followed by a simulated annealing refinement as implemented in PHENIX⁵⁵ to avoid model bias. Zinc ions were placed on the basis of an anomalous

difference map calculated with FFT.⁵⁶ The models were refined by several cycles of model corrections with COOT⁵⁷ and reciprocal space refinement with REFMAC5.⁵⁸ Final refinement steps included TLS parametrization. Water molecules were incorporated manually with COOT. Figures were generated with PyMOL.⁵⁹ Models were validated with MolProbity⁶⁰ and deposited to the Protein Data Bank (PDB) with accession numbers 4LZU and 4LZV. The structures of BLG crystallized in the presence of YCl_3 (PDB codes 3PH5 and 3PH6) were determined in our previous work.³⁶

RESULTS

Phase Behavior of BLG in the Presence of ZnCl_2 and YCl_3 . The experimental phase diagram for BLG with ZnCl_2 at room temperature is shown in Figure 1A. For comparison, the

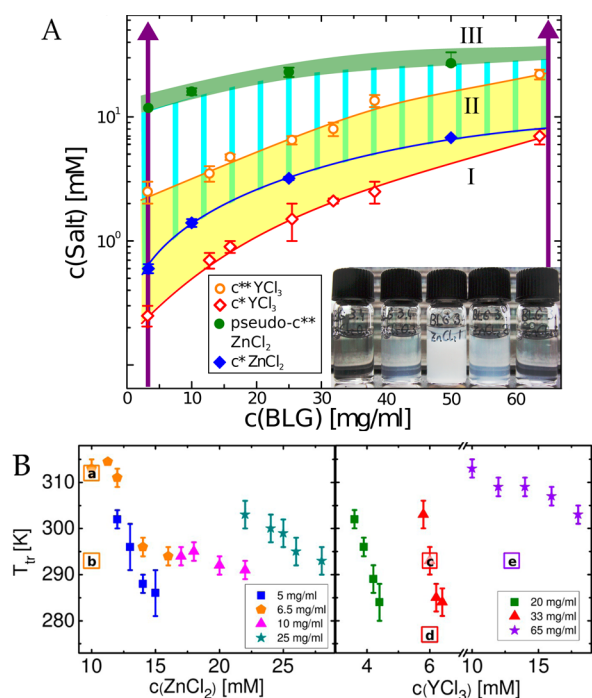


Figure 1. (A) Experimental phase diagram of BLG with ZnCl_2 and YCl_3 . In both cases, a reentrant condensation (RC) phase behavior was observed. Purple arrows mark the conditions for SAXS measurements. Inset: Photos of a series of samples with a BLG concentration of 3.4 mg/mL and increasing ZnCl_2 concentrations (from left to right: 0.1 mM, 0.3 mM, 1 mM, 20 mM, and 50 mM). (B) Transition temperature of BLG in the presence of ZnCl_2 or YCl_3 . [a–e] mark samples for the study of crystal growth in the following.

phase boundaries for BLG with YCl_3 are also shown. Upon adding ZnCl_2 , BLG solutions exhibit a distinct transition (c^*) from a clear solution in regime I to a turbid state with increasing salt concentrations (regime II). By increasing the salt concentration further, the solution became (partially) clear again (regime III); see Figure 1A, inset. In contrast to YCl_3 , where above c^{**} solutions become completely clear,^{30,31} protein solutions with ZnCl_2 remain partially turbid judged by visual inspection. This incomplete transition to a clearer state was therefore denoted as *pseudo- c^{**}* and is rather a zone than a sharp boundary. In comparison to YCl_3 , both transitions are shifted to higher salt concentration when ZnCl_2 is used. It is worth noting that this phase behavior in the presence of ZnCl_2 and also in the presence of CdCl_2 —with very similar positions of the boundaries—was observed for BLG only, but not for bovine or human serum albumin (BSA or HSA, data not

shown), where a RC phase behavior was observed in the presence of trivalent salts.^{30,31} Interestingly, the size of the ions seems to play no decisive role here, although smaller ions of the same valency have a larger charge density. These observations may indicate a more specific interaction between the divalent ions and BLG.

Previous work³⁶ showed a strongly temperature-dependent behavior for solutions of BLG with YCl_3 near c^{**} . At higher temperatures, the samples were clear and thus in regime III. Upon cooling, they became turbid below a transition temperature T_{tr} . Similar behavior was also observed in the presence of ZnCl_2 (Figure 1B) for samples within the *pseudo- c^{**}* zone. T_{tr} decreases linearly with increasing salt concentration for both salts.

Temperature-Dependent Crystallization of BLG in the Presence of ZnCl_2 and YCl_3 . Crystals were observed in the second regime of Figure 1A with both ZnCl_2 and YCl_3 . Using optical microscopy, we followed the crystallization procedure of BLG with different salt concentrations (ZnCl_2) at different temperatures. Close to (either slightly above or below) c^* , our observations suggest that the crystallization follows the classical one-step pathway; i.e., crystals nucleate directly from a supersaturated solution and grow larger without any visible cluster or LLPS phase, similar to experiments with YCl_3 .³⁶ Under our experimental conditions, this crystallization pathway did not depend on the crystallization temperature.

Close to (*pseudo- c^{**}*) (i.e., the second boundary for both ZnCl_2 and YCl_3), different growth processes depending on temperature were observed. A typical example is shown in Figure 2 for a sample close to its transition temperature (6.5

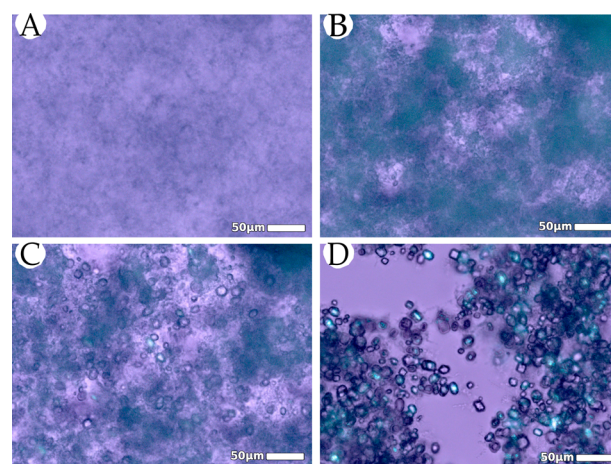


Figure 2. Typical crystallization pathway in the *pseudo- c^{**}* zone near T_{tr} . Crystals grown at 312 K: 6.5 mg/mL BLG with 10 mM ZnCl_2 . (A) Directly after preparation at 313 K. (B–D) After 7, 10, and 24 h, respectively.

mg/mL BLG and 10 mM ZnCl_2 at 312 K $\sim T_{tr}$, [a] in Figure 1B). No macroscopic LLPS was visible, but massive amorphous clusters appeared before crystallization. The amorphous clusters are metastable with respect to the crystals: they dissolved and disappeared at the end of crystallization.

For the same sample at 293 K, well below T_{tr} (Figure 3, label [b] in Figure 1B), a different growth process was observed. With time, a network of clusters forms and further relaxes into a liquid-like structure, similar to the viscoelastic behavior described in the literature for polymers and for lysozyme.^{61–63}

On the basis of the fact that these areas are growing and

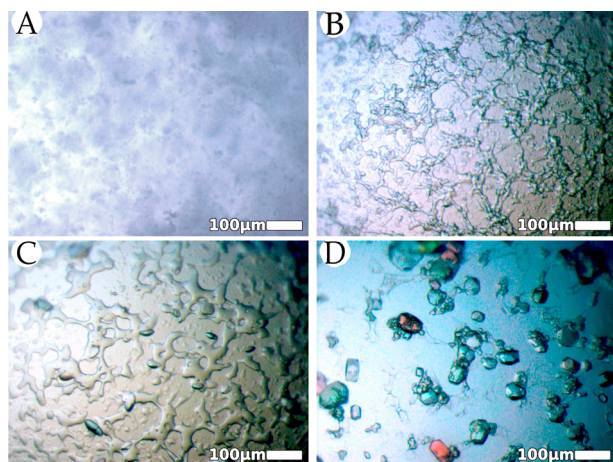


Figure 3. Typical crystallization pathway in the *pseudo-c*** zone below T_{tr} . Crystals grown at 293 K at the liquid-glass interface: 6.5 mg/mL BLG with 10 mM $ZnCl_2$. (A) Turbid sample directly after preparation. (B) Network-like dense liquid structure after 2 h. (C) After 7 h, the dense regions grew and crystals were visible. (D) After 24 h, crystal growth had consumed all dense liquid material.

merging, we conclude that they are liquid, not gel. By focusing on different depths of the sample solution, one could see that this structure forms predominantly at the lower glass interface. However, this is mainly due to the higher density of the liquid-like network structure instead of preferential wetting on the glass slide as demonstrated by the hanging drop experiments (see Supporting Information, Figure S1). Furthermore, crystal growth mainly starts from the interface between the dense and the dilute liquid phases. During crystal growth, the dense liquid phase is consumed.

Previously, we were able to show the strong dependence of protein crystallization on salt concentration (YCl_3) and temperature.³⁶ Here, we give an example of the same sample near c^{**} that follows different pathways by varying temperatures below T_{tr} , similar to the experiments with $ZnCl_2$ described above. In Figure 4, the crystal growth process of a

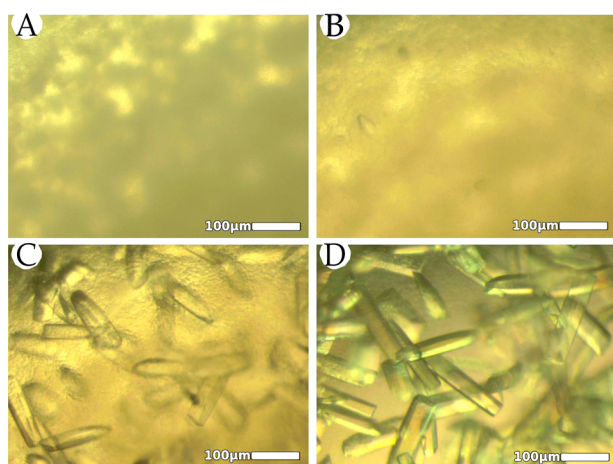


Figure 4. Pictures originate from samples prepared by the hanging drop method without prior centrifuging. Crystal growth at 293 K with a protein concentration of 33 mg/mL and 6.0 mM YCl_3 , close to the transition temperature. No liquid phase was visible but turbidity caused by large clusters. (A) After 3.5 h. (B) After 75 h. (C) After 101 h. (D) After 165 h.

sample with 33 mg/mL BLG and 6.0 mM YCl_3 at 293 K (labeled [c] in Figure 1B) is shown. This temperature is close to T_{tr} , and the sample was slightly turbid at first, but no macroscopic LLPS was visible (Figure 4A). Crystallization occurred after about 3 days (Figure 4B). With crystal growth, the turbid solution became clear and only crystals were visible in the end. No crystal growth was observed at temperatures above T_{tr} . Well below T_{tr} , another process was observed (Figure 5). When quenched to 277 K (sample [d]), the solution

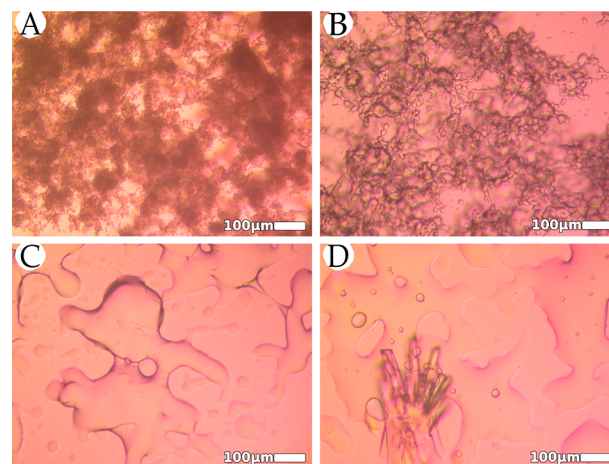


Figure 5. Formation of droplets at the sample-glass interface in a cuvette and crystal growth at 277 K. The sample has a concentration of 33 mg/mL BLG and 6.0 mM YCl_3 . (A) Directly after preparation: turbid sample. (B) After 2 h: fine liquid network. (C) After 23 h: large dense liquid regions. (D) After 54 h: crystals.

becomes turbid quickly and massive amorphous clusters are clearly visible (Figure 5A). With time, these clusters formed a liquid network (Figure 5B,C). Crystal growth was observed mainly at the interfaces, and the dense liquid-like network is consumed in the end. A similar crystallization pathway was also observed for samples with higher protein concentrations. An example is shown in Figure 1B. The sample contained 65 mg/mL BLG and 13 mM YCl_3 , and the transition temperature is about $T_{tr} = 310$ K. When crystallized at 293 K (sample [e]), a liquid-like network as an intermediate step was observed (shown in the Supporting Information, Figure S2). This behavior is very similar to that observed in Figure 3.

The crystallization procedures at different temperatures are inconsistent with the classical nucleation theory. The appearance of an intermediate phase (macroscopic LLPS or microscopic clusters) before crystallization indicates that an additional free energy minimum exists in between the supersaturated solution and the final crystalline state. Since the resolution of the optical microscope used in this work cannot distinguish whether the nucleation starts directly from the dense liquid phase or the cluster phase (or rather takes place as heterogeneous nucleation at the droplet surface), we simply denote the observed crystallization processes as different *nonclassical* pathways. The interesting observation here is that for the same sample below the transition temperature, depending on the depth of quench, the intermediate phase of the crystallization can be microscopic clusters or macroscopic LLPS. The physical mechanism of this observation will be discussed after the structural analysis of the resulting crystals.

Effective Protein-Protein Interactions Revealed by SAXS. SAXS was used to characterize the effective interactions

in protein solutions under conditions similar to the crystallization conditions. We first determined the form factors of proteins in different regimes using samples with low protein concentration, i.e., 3.3 mg/mL (Figure 6A). At very low salt

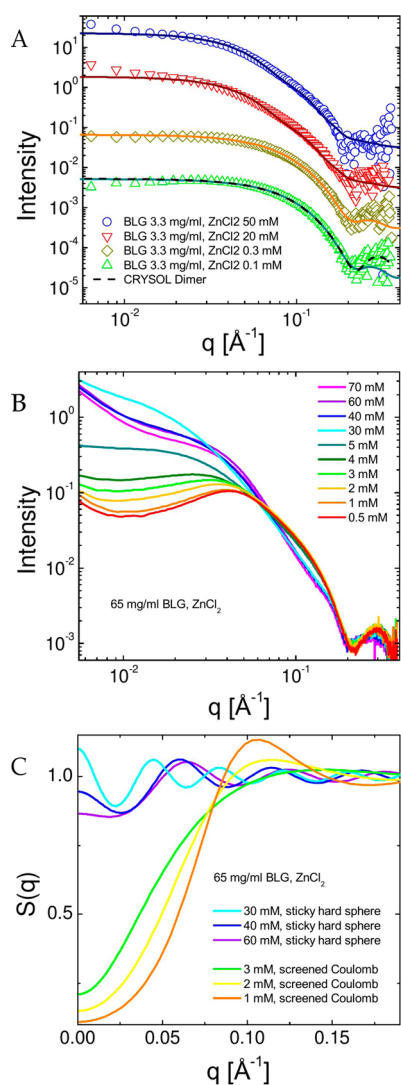


Figure 6. SAXS measurements at 3.3 and 65 mg/mL BLG with various ZnCl_2 concentrations. For better visibility, the curves were shifted in intensity and only every third data point is shown. (A) Fitted form factors for 3.3 mg/mL BLG (continuous lines: ellipsoid form factor, dashed line: form factor from crystal structure). (B) SAXS measurements at 65 mg/mL BLG with ZnCl_2 concentrations in the first and third regime. (C) Calculated structure factor of 65 mg/mL BLG with part of the ZnCl_2 concentrations from B.

concentrations, the SAXS data can be well fitted using the crystal structure of the BLG dimer (PDB code of 1BEB) using CRY SOL,⁴⁸ which can be simplified by an ellipsoid form factor with axis $a = 38 \text{ \AA}$ and $b = 19 \text{ \AA}$. The respective fitting parameters are shown in the Supporting Information, Table S1. It was found that the values of a and b were nearly constant and $a > b$ in the first regime (i.e., for 0.1 and 0.3 mM ZnCl_2). With 20 and 50 mM ZnCl_2 , the values of b became larger and $a < b$, indicating the formation of oblate-like clusters in the third regime. The minimum in scattering intensity at a q of $\sim 0.18\text{--}0.25 \text{ \AA}^{-1}$ in Figure 6A and B is dominated by the form factor. This is in contrast to the data from BLG solutions in the

presence of YCl_3 ,³⁷ where a peak was observed at 0.22 \AA^{-1} that was assigned to the monomer–monomer correlation within the clusters. The reason for this difference may be the stronger bridging effect of yttrium in comparison to zinc as explained in the following section.

Samples in the condensed regime were also measured, but due to the precipitation of proteins, these results were not used for further analysis.

SAXS data for samples with higher protein concentrations were analyzed for the effective interactions. Figure 6B,C present the SAXS data and calculated structure factor for samples with 65 mg/mL BLG and various salt concentrations. The corresponding c^* and *pseudo-c*** are around 7 mM and 30 mM, respectively. At low salt concentrations, i.e., well below c^* , the SAXS data can be well described by a combination of an ellipsoid form factor and a screened Coulomb structure factor,^{64,65} indicating repulsive interactions between protein molecules. The strength of repulsion decreases with increasing salt concentration and the fitted surface charge continuously decreases upon approaching c^* (Supporting Information, Table S2). In the third regime, an ellipsoid form factor with a sticky hard sphere structure factor was used,⁶⁶ which represents a short-ranged attractive interaction potential. The obtained volume fractions are close to the calculated value, and the interaction strength decreases if the salt concentration is further increased from *pseudo-c***.

In summary, our SAXS measurements suggest that the effective interactions are repulsive and dominated by the surface charges of proteins at low salt concentrations (ZnCl_2). With increasing salt concentration, the repulsive potential is reduced and the potential becomes attractive approaching c^* . In the third regime, the effective interactions are still attractive but decrease in strength with increasing salt concentration in good agreement with the visual observation that the solutions become less turbid. Because the attractions in the condensed regime are too strong for the growth of high quality crystals, the SAXS measurements indicate that the optimized conditions of crystallization would be near the two boundaries. These results are consistent with previous studies of BLG solutions in the presence of YCl_3 .³⁷

Crystal Structures and the Role of Multivalent Metal Ions. We determined the structures of two crystals (BLG-Zn-20, BLG-Zn-2) to resolutions of 2.44 and 2.40 \AA , respectively, including the zinc positions that could be determined unequivocally. Both crystals belong to space group $P3_221$ and contain one monomer in the asymmetric unit. The 2-fold axis of the biological dimer is aligned with the crystallographic axis. Although the same space group has been reported for BLG crystals earlier,⁶⁷ this crystal form is new and differs in the unit cell dimensions. The crystal packing of BLG with zinc ions is shown in Figure 7A. Data collection and refinement statistics of both structures are given in the Supporting Information, Tables S3 and S4.

The positions of zinc ions were determined by an anomalous density map using the Bijvoet differences as Fourier coefficients, and relative occupancies were determined during the refinement process. In both cases, one crystal contact is mediated by a zinc ion. Furthermore, a different number of additional zinc ion binding sites is not contributing to the crystal lattice formation.

The analysis of the cation binding sites in BLG-Zn-2 shows that the crystal contact is mediated by a zinc ion (zinc 1 in Figure 7), which is coordinated by residues D53 and E74 from

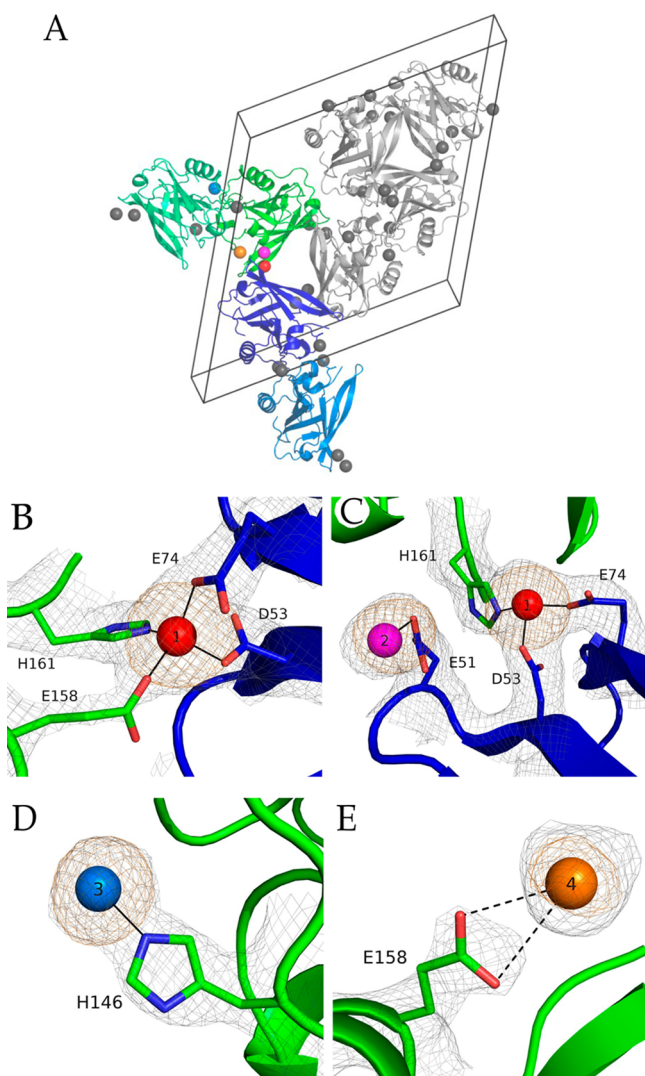


Figure 7. (A) Crystal packing of BLG crystallized with 2 mM and 20 mM ZnCl_2 . Two representative dimers are colored blue and green. Asymmetric units are represented by different color shades. Other monomers in the unit cell are represented in gray. Zinc ions are presented as gray spheres. Representative zinc ions are colored red (zinc ion mediating the crystal contact of the two representative dimers) and blue. Additional zinc sites identified in BLG-Zn-20 exclusively are colored magenta and orange. (B–F) Cation binding sites in BLG-Zn-2 (B) and BLG-Zn-20 (C–E). Density maps were calculated with FFT.⁵⁶ Sigma levels of the maps are $\sigma = 1.0$ for $2F_{\text{obs}} - F_{\text{calc}}$ maps (gray) and $\sigma = 4.0$ for anomalous maps (orange). Zinc 4 is not included into the coordinates due to its long binding distances.

one protomer and E158 and H161 from a symmetry related protomer (Figure 7B). An additional zinc binding site is found at H146, without mediating a crystal contact. In contrast to the fully occupied zinc 1 binding site, this site is only partially occupied (30%) at a concentration of 2 mM ZnCl_2 . An image is found in Supporting Information in Figure S4.

The zinc ions in BLG-Zn-20 mediating a crystal contact are coordinated by the same residues found in BLG-Zn-2 with the exception of E158 (Figure 7C). This residue is located at a different position. The zinc binding site at H146 (shown in Figure 7D) is found in BLG-Zn-20 as well, but the occupancy is higher (75%) compared to BLG-Zn-2, which is in good agreement with the ZnCl_2 concentration. Furthermore, 3.3 Å away from the carboxy group of E158, a peak in the anomalous

map indicates the presence of an additional zinc site. Modeling of a zinc ion with low occupancy resulted in long binding distances to E158 (shown in Figure 7E), which indicates a very loose metal binding site and was therefore not included in the final structure coordinates. A second additional binding site can be found at E51 with an occupancy of ca. 70% (shown in Figure 7C).

A packing analysis of both structures was performed by PISA.⁶⁸ In addition to the dimeric interface, which buries solvent accessible areas of 514 Å² and 590 Å² for BLG-Zn-2 and BLG-Zn-20, respectively, additional proteinaceous contacts build up the crystal lattice ranging from 35 Å² to 278 Å². In the case of 2 mM ZnCl_2 , the crystal contact mediated by zinc 1 has an interface of 73 Å² and in the case of 20 mM ZnCl_2 , the area has a size of 77 Å². For the additional zinc binding sites, the interface areas are 42 Å² for zinc 2 in the structure with 2 mM ZnCl_2 and 40 Å² and in the case of 20 mM ZnCl_2 39 Å² for zinc 2 and 3, respectively.

In a previous study, we determined structures of BLG crystallized in the presence of different concentrations of YCl_3 on the basis of its phase diagram (PDB codes 3PH5 and 3PH6, ref 36). We reported four yttrium ions in the BLG-Y structures, and all of them were coordinated by acidic side chains and contribute to the lattice formation. One yttrium site (yttrium 4) showed substantially lower occupancy when lower concentrations of YCl_3 were applied in the crystallization process. BLG-Zn crystals share some similarities with BLG-Y but also strong differences. As in BLG-Y, the bridging metal ions in BLG-Zn are coordinated mainly by acidic side chains, which is obvious, as acidic side chains compensate for the positive charge of the metal ions. In BLG-Zn, zinc ions are moreover coordinated by histidine residues, e.g., H161 at zinc 1. Coordination of zinc by histidine side chains is frequently observed in nature, e.g., in the family of zinc finger proteins (ref 69). In contrast to BLG-Y, where four sites built up a three-dimensional crystal lattice, we identified a single zinc ion contributing to the lattice formation (Figure 7B, Table 1).

Table 1. Comparison of BLG-Y and BLG-Zn Structure

| | space group | binding sites | bridging sites |
|--------|--------------|---------------|----------------|
| BLG-Y | $P2_12_12_1$ | 4 | 4 |
| BLG-Zn | $P3_221$ | 4 | 1 |

Another zinc site was identified, coordinated solely by H146 (Figure 7D), and it did not contribute to protomer-to-protomer interactions. Interestingly, this site revealed a concentration-dependent effect similar to yttrium 4 in BLG-Y. Moreover, at higher zinc concentrations an additional metal ion was identified. A highly speculative explanation for the reduced amounts of bridging metal ions might be found in the decreased Lewis acid character of zinc ions compared to yttrium ions, which might hamper the intermolecular bridging effect. This is in good agreement with the observation that main crystal contacts in BLG-Zn derive from proteinaceous interactions. In summary, crystallographic analysis indicates that the bridging effect of high valency metal ions promotes new protein contacts and stabilizes crystal lattice with both metal salts.

DISCUSSION

We have determined the phase behavior of the globular protein BLG in the presence of the divalent salt ZnCl_2 . The phase

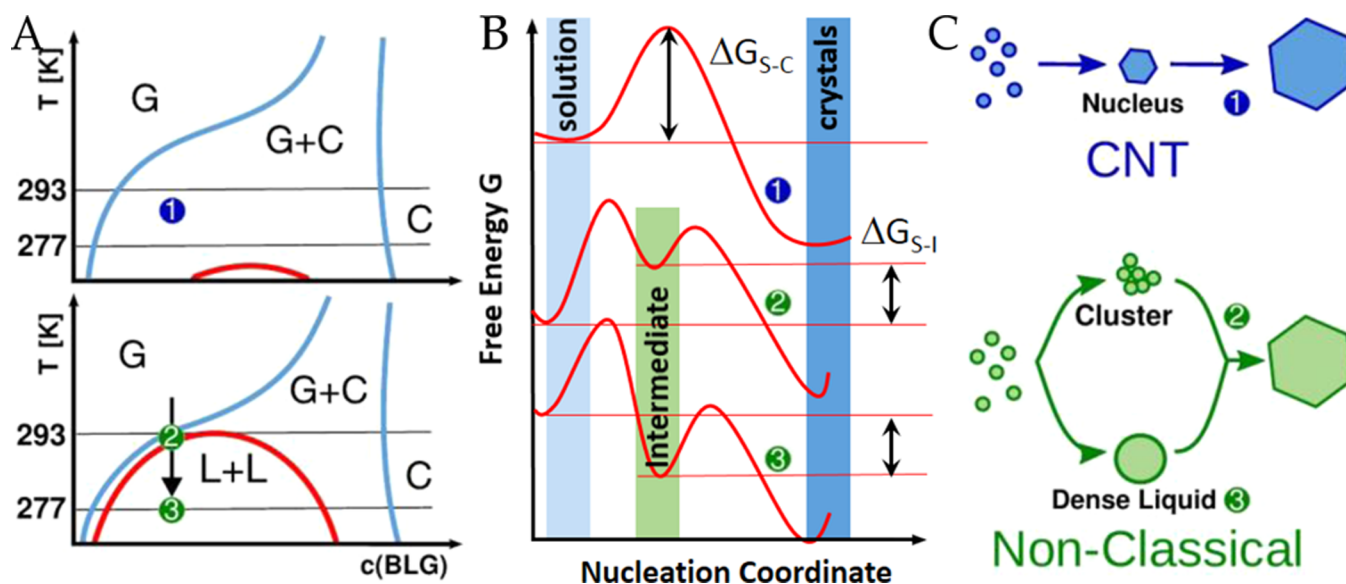


Figure 8. (A) Possible location of investigated samples in a typical phase diagram (T, c plane) for colloidal systems with a short-range attraction. Samples near c^* may have a metastable LLPS region far below the G–C boundary, whereas samples near $pseudo-c^{**}$ have a LLPS region very close to the G–C boundary (in both BLG–Y and BLG–Zn). Adapted and modified from ref 7. (B) Free energy landscape of the different crystallization pathways. The additional minimum corresponds to the formation of intermediate phases during the nonclassical crystallization. Adapted and modified from ref 3. (C) Summary of the observed crystallization pathways. “Path-1” represents the classical one-step pathway which is followed by samples near c^* . “Path-2” and “Path-3” represent nonclassical pathways with an intermediate phase of protein clusters and macroscopic LLPS, respectively, that are followed close to $pseudo-c^{**}$. Note that these nonclassical pathways are not necessarily the same as the “two-step” mechanism proposed in theory.² Details are discussed in the text.

behavior is similar to that observed for BLG solutions in the presence of trivalent salts, such as YCl_3 . However, the RC behavior in the presence of $ZnCl_2$ is not generally found for other acidic proteins examined, such as BSA and HSA. Despite this specificity, the solutions near the second phase boundary show similar temperature-dependent phase transitions. Moreover, while crystallization follows the classical one-step pathway near c^* with both salts, the crystal growth near $pseudo-c^{**}$ follows nonclassical pathways depending on the crystallization temperature. These findings and their possible interpretation are summarized in Figure 8. In the following, we discuss our experimental observations based on the established phase behavior in model colloidal systems.

Colloidal systems with short-range attraction exhibit a phase diagram (T, c) with a metastable LLPS.⁷ Although such a phase diagram is to be determined for the investigated systems, the observed temperature-dependent intermediate phases can still be explained using Figure 8A. At salt concentrations close to c^* (top), the crystallization follows a classical one-step process and does not depend strongly on temperature. The hidden LLPS, if it exists, is far below the gas–crystal (G–C) phase boundary (outside the observed temperature range) under these conditions. Lowering the temperature for crystallization within the G–C region does not change the nucleation behavior. This pathway is labeled as “1”. At high salt concentrations, close to $pseudo-c^{**}$ (bottom), the existence of an intermediate phase suggests that the liquid–liquid (L + L) coexistence region is very close to the G–C phase boundary. When quenching the solution only slightly below the transition temperature, the sample is in the state labeled as “2” in the sketched phase diagram. This position is slightly below the G–C boundary, but importantly, it is also very close to the binodal of LLPS. Under these conditions, density fluctuations lead to the formation of a microscopic protein cluster phase before crystal nucleation

occurs. This scenario (“Path-2”) is shown in Figures 2 and 4. At higher temperature, the gas phase region is reached and no crystallization can be found anymore. If the sample is quenched deeper, i.e., to location “3” which is well below the LLPS boundary, then macroscopic metastable LLPS occurs as the intermediate phase before nucleation. This scenario (“Path-3”) has been shown in Figure 3 and 5.

The corresponding free energy landscapes of these three pathways are described in Figure 8B. In the classical pathway associated with “Path-1”, there is one free energy maximum, an energy barrier that has to be overcome in order to nucleate. The free energy landscapes of the nonclassical pathways show an additional minimum corresponding to the intermediate phase. If the free energy of the intermediate phase is higher than the free energy of the initial solution, the intermediate phase is unstable and consists of mesoscopic clusters. This could be the case for samples close to the LLPS boundary like “Path-2”. If the free energy of the intermediate phase is lower than that of the initial solution, the metastable phase is a macroscopic dense liquid phase, e.g., “Path-3”. This has been summarized in ref 3.

In Figure 8C, the observed crystallization pathways are illustrated. For samples prepared close to c^* , nucleation occurs directly in the supersaturated solution with no intermediate structure or phase transition. This classical pathway is referred to as “Path-1”. Near $pseudo-c^{**}$, two different nonclassical pathways are observed depending on the crystallization temperature. “Path-2” describes the crystallization of samples located near the LLPS binodal in Figure 8A where density fluctuations lead to the microscopic clusters before nucleation. “Path-3” describes that protein solutions first undergo a macroscopic LLPS as it locates deep inside of the LLPS region before crystallization starts. However, the existence of an intermediate phase does not mean that the nucleation occurs

within protein clusters or the dense liquid phase. Our observations as well as other experimental studies¹¹ suggest that crystallization takes place rather at the interface of dense and dilute regions than within the dense phase. These nonclassical pathways observed experimentally are not the same as the two-step process first predicted by ten Wolde and Frenkel.² The theoretically predicated “two-step” mechanism describes one nucleation event in which the two order parameters (density and structure) develop in two different time scales; i.e., the supersaturated solutes first undergo a density development and form clusters or macroscopic coexistent liquid phases. In the second, subsequent step, the clusters or the dense liquid phase with already higher density undergoes a structure change and completes the nucleation event. In practice, however, another nonequilibrium phase behavior in the dense phase, i.e., gelation, may prevent the second step of structure formation as any conformation change in a gel state will be extremely slow.

On the other hand, when looking at the phase diagram in Figure 8A (bottom), because the G–C and L–L phase boundaries are very close, samples located in this region face two potential phase transitions, i.e., both crystallization and LLPS. Kinetically, LLPS occurs faster than crystal nucleation as the corresponding energy barrier is lower. Energetically, LLPS is metastable with respect to the crystalline state. From this point of view, one cannot completely rule out the possibility of two parallel classical phase transitions. Further studies should focus on real-time characterization of the role of the intermediate phase on the nucleation process, the early nucleation, and growth kinetics of such a nonclassical crystallization process.

CONCLUSION

We have studied the influence of the di- and trivalent electrolytes ZnCl_2 and YCl_3 on protein (BLG) crystallization on levels from macroscopic phase behavior to the effective intermolecular interactions and further down to the atomic crystal structures.

A reentrant condensation phase behavior has been observed in protein solutions with both salts; i.e., a condensed regime exists between c^* and $\textit{pseudo-c}^{**}$. The reentrant effect is weaker with ZnCl_2 , which might be mainly due to its lower valency compared to YCl_3 and other trivalent salts. SAXS measurements indicate that both salts can tune the effective protein–protein interaction from repulsive to attractive by crossing c^* . Above $\textit{pseudo-c}^{**}$, the interactions are still attractive but decrease with further increasing salt concentration. The effective attractions near c^* and $\textit{pseudo-c}^{**}$ provide the optimum conditions for protein crystallization.

Crystal growth in these areas followed by optical microscopy show different scenarios: while crystal growth near c^* follows a classical one-step pathway, two different nonclassical pathways are observed close to $\textit{pseudo-c}^{**}$ depending on the crystallization temperature. If the crystallization temperature is close to the transition temperature, the intermediate phase is a microscopic cluster phase. If the sample is quenched well below the transition temperature, the intermediate phase corresponds to a macroscopic LLPS. These temperature-dependent nonclassical pathways are discussed based on the phase behavior of colloidal systems with a short ranged attraction where a metastable LLPS region exists below the G–C coexistence line. Furthermore, crystallographic analysis of the resulting high

quality protein single crystals demonstrates that the multivalent metal ions provide new contacts within the lattice via bridging.

ASSOCIATED CONTENT

Supporting Information

Figure S1: Hanging drop experiment of a sample with 6.5 mg/mL BLG and 10 mM ZnCl_2 . Figure S2: Crystal growth at 293 K and a protein concentration of 65 mg/mL with 13 mM YCl_3 . Table S1: Fitting parameters of the SAXS analysis with a BLG concentration of 3.3 mg/mL. Figure S3: Fitted combination of form and structure factors for 65 mg/mL BLG in the first (A) and in the third regime (B). Table S2: Fitting parameters of the SAXS analysis with a BLG concentration of 65 mg/mL. Figure S4: Additional Zn binding site at H146 in BLG–Zn-2. This material is available free of charge via the Internet at <http://pubs.acs.org>.

AUTHOR INFORMATION

Corresponding Authors

*E-mail: fajun.zhang@uni-tuebingen.de

*E-mail: thilo.stehle@uni-tuebingen.de

Notes

The authors declare no competing financial interest.

ACKNOWLEDGMENTS

We gratefully acknowledge the financial support from DFG and the allocation of beamtime as well as the support of the beamline scientists at SLS, ID02 (ESRF), and PETRA III. A.S. acknowledges a fellowship of the Landesgraduiertenförderung. The authors thank Hans-Joachim Schöpe for valuable discussions and comments.

REFERENCES

- (1) Durbin, S.; Feher, G. Protein crystallization. *Annu. Rev. Phys. Chem.* **1996**, *47*, 171–204.
- (2) ten Wolde, P. R.; Frenkel, D. Enhancement of Protein Crystal Nucleation by Critical Density Fluctuations. *Science* **1997**, *277*, 1975–1978.
- (3) Vekilov, P. G. Dense Liquid Precursor for the Nucleation of Ordered Solid Phases from Solution. *Cryst. Growth Des.* **2004**, *4*, 671–685.
- (4) Gebauer, D.; Clfen, H. Prenucleation clusters and non-classical nucleation. *Nano Today* **2011**, *6*, 564–584.
- (5) Wallace, A. F.; Hedges, L. O.; Fernandez-Martinez, A.; Raiteri, P.; Gale, J. D.; Waychunas, G. A.; Whitlam, S.; Banfield, J. F.; De Yoreo, J. J. Microscopic Evidence for Liquid-Liquid Separation in Supersaturated CaCO_3 Solutions. *Science* **2013**, *341*, 885–889.
- (6) Sear, R. P. The non-classical nucleation of crystals: microscopic mechanisms and applications to molecular crystals, ice and calcium carbonate. *Int. Mater. Rev.* **2012**, *57*, 328–356.
- (7) Anderson, V. J.; Lekkerkerker, H. N. W. Insights into phase transition kinetics from colloid science. *Nature* **2002**, *416*, 811–815.
- (8) Sear, R. Nucleation at contactmeet solid surfaces lineswhere fluidfluid interfaces. *J. Phys.: Condens. Matter* **2007**, *19*, 466106.
- (9) Galkin, O.; Vekilov, P. G. Control of protein crystal nucleation around the metastable liquid–liquid phase boundary. *Proc. Natl. Acad. Sci. U.S.A.* **2000**, *97*, 6277–6281.
- (10) Galkin, O.; Vekilov, P. G. Are Nucleation Kinetics of Protein Crystals Similar to Those of Liquid Droplets? *J. Am. Chem. Soc.* **2000**, *122*, 156–163.
- (11) Chen, Q.; Vekilov, P. G.; Nagel, R. L.; Hirsch, R. E. Liquid-Liquid Phase Separation in Hemoglobins: Distinct Aggregation Mechanisms of the $\beta 6$ Mutants. *Biophys. J.* **2004**, *86*, 1702–1712.
- (12) Gebauer, D.; Völkel, A.; Cölfen, H. Stable prenucleation calcium carbonate clusters. *Science* **2008**, *322*, 1819–22.

- (13) Harland, J. L.; Henderson, S. I.; Underwood, S. M.; van Megen, W. Observation of Accelerated Nucleation in Dense Colloidal Fluids of Hard Sphere Particles. *Phys. Rev. Lett.* **1995**, *75*, 3572–3575.
- (14) Martin, S.; Bryant, G.; van Megen, W. Crystallization kinetics of polydisperse colloidal hard spheres: Experimental evidence for local fractionation. *Phys. Rev. E* **2003**, *67*, 061405.
- (15) Martin, S.; Bryant, G.; van Megen, W. Crystallization kinetics of polydisperse colloidal hard spheres. II. Binary mixtures. *Phys. Rev. E* **2005**, *71*, 021404.
- (16) Schöpe, H. J.; Bryant, G.; van Megen, W. Two-Step Crystallization Kinetics in Colloidal Hard-Sphere Systems. *Phys. Rev. Lett.* **2006**, *96*, 175701.
- (17) Schilling, T.; Schöpe, H. J.; Oettel, M.; Opletal, G.; Snook, I. Precursor-Mediated Crystallization Process in Suspensions of Hard Spheres. *Phys. Rev. Lett.* **2010**, *105*, 025701.
- (18) Gliko, O.; Pan, W.; Katsonis, P.; Neumaier, N.; Galkin, O.; Weinkauf, S.; Vekilov, P. G. Metastable Liquid Clusters in Super- and Undersaturated Protein Solutions. *J. Phys. Chem. B* **2007**, *111*, 3106–3114.
- (19) Pan, W.; Galkin, O.; Filobelo, L.; Nagel, R. L.; Vekilov, P. G. Metastable Mesoscopic Clusters in Solutions of Sickle-Cell Hemoglobin. *Biophys. J.* **2007**, *92*, 267–277.
- (20) Pan, W.; Vekilov, P. G.; Lubchenko, V. Origin of anomalous mesoscopic phases in protein solutions. *J. Phys. Chem. B* **2010**, *114*, 7620–30.
- (21) Hutchens, S. B.; Wang, Z.-G. Metastable cluster intermediates in the condensation of charged macromolecule solutions. *J. Chem. Phys.* **2007**, *127*, 084912.
- (22) Li, Y.; Lubchenko, V.; Vorontsova, M. a.; Filobelo, L.; Vekilov, P. G. Ostwald-like ripening of the anomalous mesoscopic clusters in protein solutions. *J. Phys. Chem. B* **2012**, *116*, 10657–64.
- (23) Sleutel, M.; Driessche, A. E. S. V. Role of clusters in nonclassical nucleation and growth of protein crystals. *Proc. Nat. Sci. U.S.A.* **2014**, *111*, E546–E553.
- (24) McPherson, A. Current approaches to macromolecular crystallization. *Eur. J. Biochem.* **1990**, *189*, 1–23.
- (25) Trakhanov, S.; Kreimer, D. I.; Parkin, S.; Ames, G. F.-L.; Rupp, B. Cadmium-induced crystallization of proteins: II. Crystallization of the Salmonella typhimurium histidine-binding protein in complex with L-histidine, L-arginine, or L-lysine. *Protein Sci.* **1998**, *7*, 600–604.
- (26) Yao, N.; Trakhanov, S.; Quiocho, F. A. Refined 1.89 Å structure of the histidine-binding protein complexed with histidine and its relationship with many other active transport/chemosensory proteins. *Biochemistry* **1994**, *33*, 4769–4779.
- (27) Newcomer, M. E.; Liljas, A.; Eriksson, U.; Sundelin, J.; Rask, L.; Peterson, P. A. Crystallization of and preliminary X-ray data for an intracellular vitamin A-binding protein from rat liver. *J. Biol. Chem.* **1981**, *256*, 8162–8163.
- (28) Schlichtkrull, J. Insulin Crystals. *Acta Chem. Scand.* **1956**, *10*, 1455–1458.
- (29) Trakhanov, S.; Quiocho, F. A. Influence of divalent cations in protein crystallization. *Protein Sci.* **1995**, *4*, 1914–1919.
- (30) Zhang, F.; Skoda, M. W. A.; Jacobs, R. M. J.; Zorn, S.; Martin, R. A.; Martin, C. M.; Clark, G. F.; Weggler, S.; Hildebrandt, A.; Kohlbacher, O.; Schreiber, F. Reentrant Condensation of Proteins in Solution Induced by Multivalent Counterions. *Phys. Rev. Lett.* **2008**, *101*, 148101.
- (31) Zhang, F.; Weggler, S.; Ziller, M. J.; Ianeselli, L.; Heck, B. S.; Hildebrandt, A.; Kohlbacher, O.; Skoda, M. W. A.; Jacobs, R. M. J.; Schreiber, F. Universality of protein reentrant condensation in solution induced by multivalent metal ions. *Proteins* **2010**, *78*, 3450–3457.
- (32) Roosen-Runge, F.; Heck, B. S.; Zhang, F.; Kohlbacher, O.; Schreiber, F. Interplay of pH and Binding of Multivalent Metal Ions: Charge Inversion and Reentrant Condensation in Protein Solutions. *J. Phys. Chem. B* **2013**, *117*, 5777–5787.
- (33) Zhang, F.; Roosen-Runge, F.; Sauter, A.; Wolf, M.; Jacobs, R. M. J.; Schreiber, F. Reentrant Condensation, Liquid-Liquid Phase Separation and Crystallization in Protein Solutions Induced by Multivalent Metal Ions. *Pure Appl. Chem.* **2014**, *86*, 191–202.
- (34) Soraruf, D.; Roosen-Runge, F.; Grimaldo, M.; Zanini, F.; Schweins, R.; Seydel, T.; Zhang, F.; Roth, R.; Oettel, M.; Schreiber, F. Protein cluster formation in aqueous solution in the presence of multivalent metal ions - a light scattering study. *Soft Matter* **2014**, *10*, 894–902.
- (35) Zhang, F.; Roth, R.; Wolf, M.; Roosen-Runge, F.; Skoda, M. W. A.; Jacobs, R. M. J.; Sztucki, M.; Schreiber, F. Charge-controlled metastable liquid-liquid phase separation in protein solutions as a universal pathway towards crystallization. *Soft Matter* **2012**, *8*, 1313–1316.
- (36) Zhang, F.; Zocher, G.; Sauter, A.; Stehle, T.; Schreiber, F. Novel approach to controlled protein crystallization through ligandation of yttrium cations. *J. Appl. Crystallogr.* **2011**, *44*, 755–762.
- (37) Zhang, F.; Roosen-Runge, F.; Skoda, M. W. A.; Jacobs, R. M. J.; Wolf, M.; Callow, P.; Frielinghaus, H.; Pipich, V.; Prevost, S.; Schreiber, F. Hydration and interactions in protein solutions containing concentrated electrolytes studied by small-angle scattering. *Phys. Chem. Chem. Phys.* **2012**, *14*, 2483–2493.
- (38) Lyklema, J. Overcharging, charge reversal: Chemistry or physics? *Colloid Surface A* **2006**, *291*, 3–12.
- (39) Verheul, M.; Pedersen, J. S.; Roefs, S. P. F. M.; de Kruijff, K. G. Association Behavior of Native β -Lactoglobulin. *Biopolymers* **1999**, *49*, 11–20.
- (40) Elofsson, U. M.; Paulsson, M. A.; Arnebrant, T. Adsorption of β -Lactoglobulin A and B in Relation to Self-Association: Effect of Concentration and pH. *Langmuir* **1997**, *13*, 1695–1700.
- (41) Sober, H. A. *CRC Handbook of Biochemistry: Selected Data for Molecular Biology*; CRC: Boca Raton, FL, 1970.
- (42) Narayanan, T. In *Soft Matter Characterization*; Borsali, R., Pecora, R., Ed.; Springer: Berlin, 2008; Chapter Synchrotron Small-Angle X-ray Scattering.
- (43) Ianeselli, L.; Zhang, F.; Skoda, M. W. A.; Jacobs, R. M. J.; Martin, R. A.; Callow, S.; Prevost, S.; Schreiber, F. Protein-protein interactions in ovalbumin solutions studied by small-angle scattering: effect of ionic strength and the chemical nature of cations. *J. Phys. Chem. B* **2010**, *114*, 3776–83.
- (44) Glatter, O.; Kratky, O. *Small Angle X-ray Scattering*; Academic Press: New York, 1982; p 515.
- (45) Svergun, D. I.; Koch, M. H. J. Small-angle scattering studies of biological macromolecules in solution. *Rep. Prog. Phys.* **2003**, *66*, 1735.
- (46) Hansen, J.-P.; McDonald, I. R. *Theory of Simple Liquids*, 3rd ed.; Academic Press: New York, 2006.
- (47) Brownlow, S.; Cabral, J. H. M.; Cooper, R.; Flower, D. R.; Yewdall, S. J.; Polikarpov, I.; North, A. C. T.; Sawyer, L. Bovine β -Lactoglobulin at 1.8 Å Resolution - Still an Enigmatic Lipocalin. *Structure* **1997**, *5*, 481–495.
- (48) Svergun, D.; Barberato, C.; Koch, M. H. J. CRY SOL - a Program to Evaluate X-ray Solution Scattering of Biological Macromolecules from Atomic Coordinates. *J. Appl. Crystallogr.* **1995**, *28*, 768–773.
- (49) Chen, S.-H. Small angle neutron scattering studies of the structure and interaction in micellar and microemulsion systems. *Annu. Rev. Phys. Chem.* **1986**, *37*, 351–399.
- (50) Ishihara, A. Determination of Molecular Shape by Osmotic Measurement. *J. Chem. Phys.* **1950**, *18*, 1446–1449.
- (51) Kline, S. R. Reduction and analysis of SANS and USANS data using IGOR Pro. *J. Appl. Crystallogr.* **2006**, *39*, 895–900.
- (52) Zhang, F.; Skoda, M. W. A.; Jacobs, R. M. J.; Martin, R. A.; Martin, C. M.; Schreiber, F. Protein Interactions Studied by SAXS: Effect of Ionic Strength and Protein Concentration for BSA in Aqueous Solutions. *J. Phys. Chem. B* **2007**, *111*, 251–259.
- (53) Kabsch, W. XDS. *Acta Crystallogr., Sect. D* **2010**, *66*, 125–132.
- (54) McCoy, A. J.; Grosse-Kunstleve, R. W.; Adams, P. D.; Winn, M. D.; Storoni, L. C.; Read, R. J. Phaser crystallographic software. *J. Appl. Crystallogr.* **2007**, *40*, 658–674.
- (55) Adams, P. D. et al. PHENIX, a comprehensive Python-based system for macromolecular structure solution. *Acta Crystallogr., Sect. D Biol.* **2010**, *66*, 213–21.

- (56) Ten, L. Crystallographic fast Fourier transforms. *Acta Crystallogr., Sect. A* **1973**, *29*, 183–191.
- (57) Emsley, P.; Lohkamp, B.; Scott, W. G.; Cowtan, K. Features and development of Coot. *Acta Crystallogr., Sect. D* **2010**, *66*, 486–501.
- (58) Murshudov, G. N.; Vagin, A. A.; Dodson, E. J. Refinement of macromolecular structures by the maximum-likelihood method. *Acta Crystallogr., Sect. D* **1997**, *53*, 240–55.
- (59) Schrödinger, L. *The PyMOL Molecular Graphics System*, Version 1.5.0.4; Schrödinger, LLC.
- (60) Chen, V. B.; Arendall, W. B., III; Headd, J. J.; Keedy, D. A.; Immormino, R. M.; Kapral, G. J.; Murray, L. W.; Richardson, J. S.; Richardson, D. C. MolProbity: all-atom structure validation for macromolecular crystallography. *Acta Crystallogr., Sect. D* **2010**, *66*, 12–21.
- (61) Kulkarni, A. M.; Dixit, N. M.; Zukoski, C. F. Ergodic and non-ergodic phase transitions in globular protein suspensions. *Faraday Discuss.* **2003**, *123*, 37–50.
- (62) Tanaka, S.; Ataka, M.; Ito, K. Pattern formation and coarsening during metastable phase separation in lysozyme solutions. *Phys. Rev. E* **2002**, *65*, 051804.
- (63) Tanaka, H.; Nishikawa, Y. Viscoelastic Phase Separation of Protein Solutions. *Phys. Rev. Lett.* **2005**, *95*, 078103.
- (64) Hayter, J. B.; Penfold, J. An analytic structure factor for macroion solutions. *Mol. Phys.* **1981**, *42*, 109–118.
- (65) Hansen, J.-P.; Hayter, J. B. A rescaled MSA structure factor for dilute charged colloidal dispersions. *Mol. Phys.* **1982**, *46*, 651–656.
- (66) Baxter, R. J. Percus–Yevick Equation for Hard Spheres with Surface Adhesion. *J. Chem. Phys.* **1968**, *49*, 2770–2774.
- (67) Qin, B. Y.; Jameson, G. B.; Bewley, M. C.; Baker, E. N.; Creamer, L. K. Functional implications of structural differences between variants A and B of bovine-lactoglobulin. *Protein Sci.* **1999**, *8*, 75–83.
- (68) Krissinel, E.; Henrick, K. Inference of macromolecular assemblies from crystalline state. *J. Mol. Biol.* **2007**, *372*, 774–97.
- (69) Schuetz, A.; Nana, D.; Rose, C.; Zocher, G.; Milanovic, M.; Koenigsmann, J.; Blasig, R.; Heinemann, U.; Carstanjen, D. The structure of the Klf4 DNA-binding domain links to self-renewal and macrophage differentiation. *Cell. Mol. Life Sci.* **2011**, *68*, 3121–3131.